ChemComm

COMMUNICATION

View Article Online
View Journal

Cite this: DOI: 10.1039/c9cc00001a

Received 1st January 2019,
Accepted 8th May 2019

DOI: 10.1039/c9cc00001a

rsc.li/chemcomm

Electrodeposition of pure phase SnSb exhibiting high stability as a sodium-ion battery anode†

Jeffrey Ma and Amy L. Prieto *

Electrodeposition of pure phase SnSb is reported for the first time. The purity of the product is important, as the impure phase is found to be detrimental to the material's lifetime as a sodium-ion anode. The directly deposited electrode was able to retain 95% capacity after 300 cycles, and only fall below 80% capacity retention after 800 cycles when cycled *versus* sodium.

Secondary batteries play a major role in energy storage as we slowly transition from non-renewable sources, such as fossil fuels, to cleaner and more sustainable storage methods. Of the secondary battery technologies, lithium-ion batteries are currently utilized in applications ranging from portable devices to all-electric vehicles. In recent years there has been an influx in the research on sodium-ion batteries as a substitute for lithium-ion in certain technologies, such as large grid storage, due to sodium's higher abundance and low cost. The traditional anode material for lithium-ion batteries, graphite, does not perform well as a sodium-ion anode.[1,2] This is due to the larger size of Na^+ ions when compared to Li^+ ions, which makes graphite not a compatible host. This motivates the need for optimal Na-ion anodes that can exhibit high capacity and long cycle life. Currently, most investigations on sodium anode materials revolve around hard carbon.[3] However, hard carbon exhibits poor cycling performance and can result in the plating and dendritic growth of sodium metal on the surface, which is a safety hazard.

The motivation in studying alloy anode materials is their greater volumetric and gravimetric capacities when compared to hard carbon. Silicon, while shown to be promising as a lithium-ion battery due to its high theoretical capacity, has demonstrated a lack of ability to store sufficient amounts of sodium.[4,5] Of all the potential alloy anode materials, Sn (847 mA h g^{-1}) and Sb (660 mA h g^{-1}) have been heavily studied due to their large theoretical capacities. Intermetallic alloys, like SnSb, have smaller volume expansions upon sodiation, resulting in longer cycle life and improved rate performances. Previous reports on SnSb have suggested that polycrystalline SnSb reforms upon cycling in lithium-ion batteries, which may have some benefits in terms of its mechanical properties.[6] Due to the inability to directly transfer knowledge of anode research from lithium-ion to sodium-ion technology, *i.e.* Si and graphite, SnSb has become a frontrunner for potential application as a sodium-ion battery anode. Ultimately, our goal is to develop an easy and scalable synthesis method with control over the composition, morphology, and surface area of the SnSb anode material, while enhancing its performance.

The bimetallic SnSb alloy has been previously synthesized using methods such as ball milling, electrospinning, hot injection, chemical reduction, solvothermal, and through traditional solid-state means.[6–11] Most of these methods require higher temperatures, which can cause heterogeneous products given the difference in vapor pressure between the two elements. All of these synthetic methods produce powders as their product, resulting in the need for binders for testing the active materials electrochemically in a battery. Here we directly electrodeposit SnSb is onto a conducting substrate at room temperature, without the need of additional binders or post processing. Electrodeposition enables control of the composition, particle size, and thickness of the material. While the first Sn–Sb lithium anode reported was synthesized *via* electrodeposition, pure phase SnSb has never been reported through this process.[12–17] The most common impurities in previous reports are Sn, Cu_2Sb, Cu_3Sn, and SnO. All of these impurities are electrochemically active. As a result, the electrodeposition of pure phase SnSb is desired in order to study how the pure phase material interacts with other components in the battery during electrochemical cycling. In this study, we have successfully synthesized pure phase SnSb by electrodeposition by using a deep eutectic solvent. Pure SnSb electrodes exhibit competitive gravimetric capacities compared to carbon with binder additives, while maintaining long cycle life in a sodium-ion battery.

Thin films of SnSb were synthesized using a solution containing Sn(II) and Sb(III) chlorides as precursors, and ethaline

Department of Chemistry, Colorado State University, Fort Collins, Colorado 80523, USA. E-mail: amy.prieto@colostate.edu

† Electronic supplementary information (ESI) available. See DOI: 10.1039/c9cc00001a

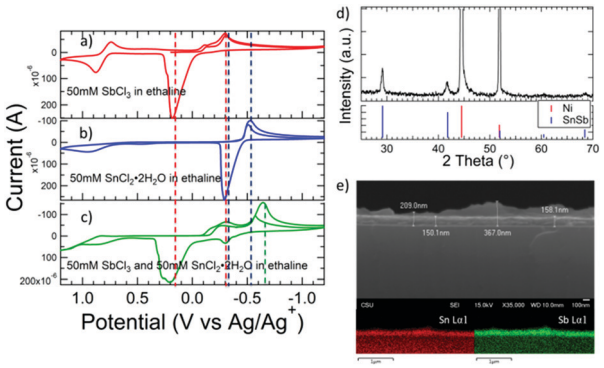

Fig. 1 Cyclic voltammograms of (a) 50 mM $SnCl_2{\cdot}2H_2O$ in ethaline and (b) 50 mM $SbCl_3$ in ethaline separately (c) 50 mM $SnCl_2{\cdot}2H_2O$ and 50 mM $SbCl_3$ in ethaline combined. A Ag wire reference and Pt working electrode were used at a scan rate of 50 mV s^{-1}. (d) XRD and (e) SEM-EDS verifying the presence of SnSb.

(1 : 2 by weight choline chloride to ethylene glycol) was used as the solvent for this electrodeposition solution. Cyclic voltammetry of the individual tin and antimony in ethaline solutions (Fig. 1a and b) and the solution containing both tin and antimony in ethaline (Fig. 1c) were examined in order to identify the potential at which co-electrodeposition of the two metals should occur. The cyclic voltammetry of the solution containing both Sn(II) chloride and Sb(III) chloride in ethaline presents two reduction peaks during its first sweep that can be identified based on the cyclic voltammetry of the individual solutions. During the first cathodic sweep, the reduction of Sb^{3+} to Sb^0 is present at −0.3 V and reduction of Sn^{2+} to Sn^0 at −0.55 V *vs.* Ag/Ag^+. During the reverse sweep of the scan direction, oxidation peaks are present at −0.3 V *vs.* Ag/Ag^+ for the stripping of Sn^0 into Sn^{2+} and 0.2 V *vs.* Ag/Ag^+ for the stripping of Sb^0 into Sb^{3+}. The more positive potential peaks at approximately 0.9 V *vs.* Ag/Ag^+ are believed to be related to the Sb^{3+}/Sb^{5+} couple. The reduction of Sb^{3+} to Sb^0 at −0.3 V and Sn^{2+} to Sn^0 at −0.55 V *vs.* Ag/Ag^+ are the crucial data needed for the electrodeposition of SnSb. Due to tin's more negative reduction potential, co-deposition of Sb and Sn should occur at a potential more negative of −0.55 V *vs.* Ag/Ag^+. The deposition potential cannot be −0.3 V *vs.* Ag/Ag^+ as the cyclic voltammetry data suggests the stripping of Sn occurs while Sb plates between −0.3 V and −0.45 *vs.* Ag/Ag^+. This oxidative current suggesting the stripping of Sn^0 into Sn^{2+} is not complete until −0.45 V. Using this data, and through optimization of electrodeposition conditions, SnSb was electrodeposited at −0.7 V *vs.* Ag/Ag^+ onto a nickel substrate. The X-ray diffraction (XRD) pattern verifies the formation of only SnSb phase onto the nickel substrate (Fig. 1d). A nickel substrate was used instead of copper due to possible detrimental migration effects of copper into the active material layer seen in a previous work.[18]

The electrochemical performance of the thin film SnSb as a sodium-ion anode was investigated using Swagelok half-cells. A standard electrolyte of 1 M $NaPF_6$ in dimethyl carbonate (DMC) with 5% by weight fluoroethylene carbonate (FEC) was used for all tested cells. Lifetime cycling studies with greater than 200 cycles are rarely seen in Sn–Sb literature,[6,19–23] which does not show the overall performance and failure of the material. As shown by the galvanostatic cycling at *C*/2 rate, the electrodeposited SnSb has higher stability and better performance than either pure Sn and Sb electrodeposited from ethaline (Fig. S1, ESI†). During its initial discharge, a significant amount of irreversible capacity is observed, which may be related to the formation of a solid–electrolyte interface (SEI) layer between the surface of the electrode and the decomposing electrolyte. However, after the initial cycle, the performance of the material begins to stabilize with a discharge capacity of 548.2 mA h g^{-1} on its second cycle. Similar to previous reports, the capacity obtained at around the *C*/2 rate is found to be in the range of 400–600 mA h g^{-1}, which is significantly less than its theoretical capacity (752 mA h g^{-1}). Others have hypothesized that this is due to the inability of tin to sodiate completely in SnSb due to a shift to higher overpotentials at this rate.[24] Based on the capacity at the second cycle, electrodeposited SnSb is found to maintain significant stability during cycling (Fig. 2) with 95% capacity retention after 300 cycles (at 520.8 mA h g^{-1}) and 90.5% capacity retention after 500 cycles (at 496.1 mA h g^{-1}). The SnSb anode retains this impressive stability over many cycles and does not fall below 80% capacity retention until after 800 cycles. This slow decrease in capacity can be connected to continuous volumetric expansion and pulverization, resulting in isolation of active material and growth of SEI on the newly exposed surface. This growth of the SEI will result in slower kinetics and eventual sudden death of the cell. This can be supported with *ex situ* SEM images taken of a SnSb electrode after cycling in a sodium-ion half-cell showing a buildup of an organic-like SEI on the electrode surface in later cycles (Fig. S2, ESI†).

Rate capability tests were also performed to test the performance of pure SnSb at different current densities (Fig. 2). The electrodeposited SnSb exhibits specific gravimetric capacities

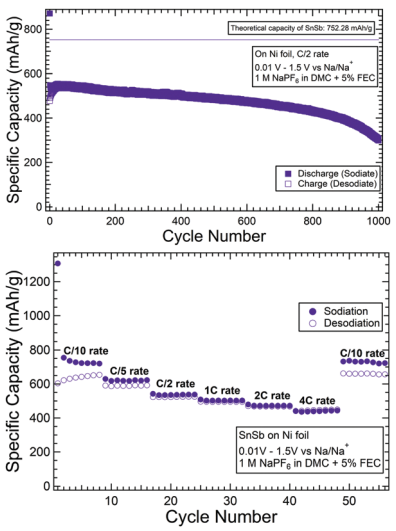

Fig. 2 Electrochemical performance of electrodeposited SnSb (top). The test was performed by galvanostatically cycling at *C*/2 rate between the potential window of 0.01 V–1.5 V in a sodium half-cell. Rate capability of electrodeposited SnSb at different current rates (bottom). The test was performed in a sodium half-cell for 8 cycles at each different rate. The potential range used was 0.01 V–1.5 V.

of 720 mA h g^{-1}, 620 mA h g^{-1}, 540 mA h g^{-1}, 500 mA h g^{-1}, 472 mA h g^{-1}, and 440 mA h g^{-1} at *C*/10, *C*/5, *C*/2, 1*C*, 2*C*, and 4*C*, respectively. After cycling at the higher rates, a cycle at *C*/10 rate shows that the electrode fully recovers with no noticeable drop in capacity, which verifies the stability of the electrode.

Using the *C*/2 rate galvanostatic cycling data, differential capacity plots were extracted for pure Sn, Sb, and SnSb phase samples (Fig. 3a–c). Unlike previous reports for SnSb in lithium-ion batteries, the electrochemistry involved with the sodiation of SnSb is not just the addition of Sn and Sb sodiation events individually. The sodiation events of SnSb occur at different potentials when compared to the electrodeposited Sn and Sb electrodes individually. Similarly to previous reports,[9] sodiation events for SnSb are seen at 0.64 V, 0.46 V, and 0.28 V with complementary desodiation events occurring at 0.6 V, 0.8 V, and 0.95 V. The sodiation event seen at ~0.01 V in SnSb when compared to the pure Sn electrode supports the hypothesis from previous reports that the inability of tin to completely sodiate in SnSb may be the reasoning as to why SnSb cannot reach its theoretical capacity at this rate.

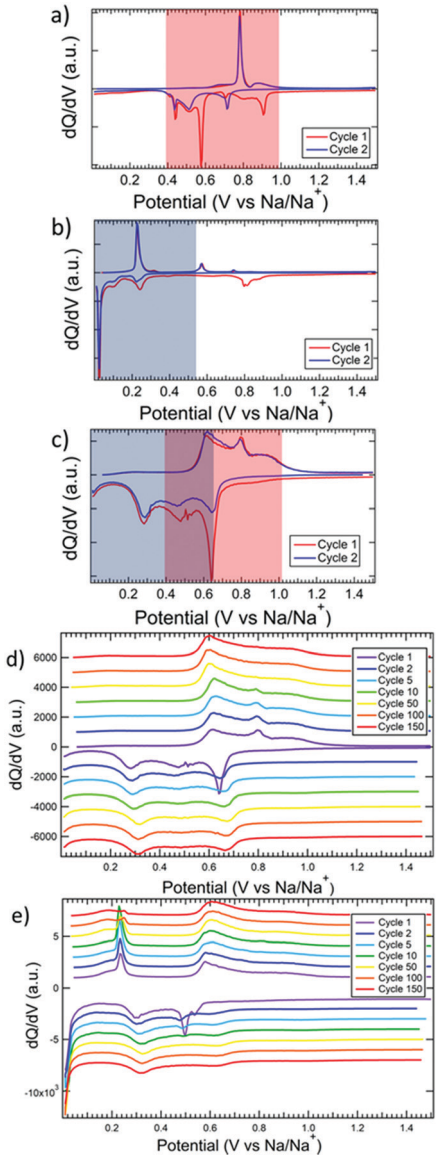

Fig. 3 Differential capacity plots of electrodeposited (a) Sb, (b) Sn and (c) SnSb showing the first two cycles. Differential capacity plots of electrodeposited (d) SnSb and (e) 50 : 50 Sn : SnSb during the 1st, 2nd, 5th, 10th, 50th, 100th, and 150th cycles, obtained from galvanostatically cycling at *C*/2 rate, within the range of 1.5 V–0.01 V *vs.* Na/Na^+.

The differential capacity plots also verify the lack of Sn impurity phases present as a result of this synthesis. Fig. 3b shows a sodiation event at 0.01 V and a desodiation event at 0.2 V that are sharp and distinct features observed when cycling at this current density in the presence of Sn and not pure phase SnSb. This observation is verified by intentionally introducing Sn impurities in a 50 : 50 Sn : SnSb electrode (Fig. 3e), where the differential capacity plot presents the defined desodiation event at 0.2 V that is not present over the different cycles at *C*/2 of pure phase SnSb (Fig. 3d). This suggests introduction of Sn impurities would ultimately increase Sn desodiation activity at 0.2 V to a more defined peak as more Sn is present in this system when cycling at this rate. Galvanostatic cycling of SnSb films containing Sn impurities also suggests that a Sn impurity is the detrimental to the electrode's cycle life (Fig. S3, ESI†).

Interestingly, our *ex situ* XRD data (Fig. 4) shows the reappearance of crystalline SnSb after the first cycle at *C*/2 rate, which previous reports did not see. Previous literature reported the disappearance of the peaks and the formation of amorphous features immediately after the first cycle.[24,25] Our work suggests the electrodeposited SnSb does reform, but gradually loses long range order and changes from crystalline SnSb to an amorphous phase with each successive cycle, unlike the immediate transformation observed in previous reports. This observation is similar to what was seen in a previous study of SnSb in lithium-ion batteries where SnSb reforms, but loses long range ordering over cycling.[6] Extended X-ray absorption and fine structure (EXAFS) from a recent report also suggests the reformation of the same SnSb phase with similar Sn and Sb environments after desodiation, but loss of long range ordering based on their data.[26] Transmission electron microscopy (TEM) and electron diffraction from a recent study also support SnSb reformation.[27] Additional experiments were performed verifying the reformation of crystalline SnSb after electrochemical cycling in our system (Fig. S4, ESI†).

To summarize, by using an ethaline-based solution the electrodeposition of pure phase SnSb has been reported for the first time. Electrodeposited SnSb, without binders and carbon additives, was tested as a sodium-ion battery anode. While long-term cycling studies over 200 cycles have rarely been previously reported in SnSb literature, we report 1000 cycles to better understand the lifetime and long cycling stability of our SnSb electrodes. Although capacity below theoretical maximum was obtained from galvanostatic cycling at *C*/2 rate, SnSb exhibited high cycling stability, falling below 80% capacity retained after 800 cycles. Rate capability tests demonstrated the stability of SnSb cycling with higher current densities. Differential capacity plots and *ex situ* XRD reveal the gradual change, instead of an immediate change as seen from previous

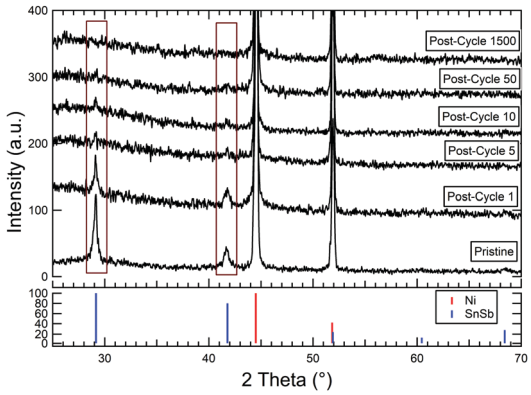

Fig. 4 *Ex situ* XRD of electrodeposited SnSb galvanostatically cycled at *C*/2 rate, within the range of 1.5 V–0.01 V *vs.* Na/Na^+.

reports, from crystalline SnSb to an amorphous phase for electrodeposited SnSb during *C*/2 cycling. The differential capacity plots also verify the purity of SnSb with absence of distinct Sn electrochemical events. This study reveals some structural integrity with the reformation of SnSb, which may be related to the electrochemical stability seen. If the reformation is important to the stability of the material, purity of the material is crucial for obtaining longer cycle lifetime of the material. The films we report here are thin, but recently, the electrochemical performance of a similar thickness material, ~200 nm Sn, was electrodeposited on a 3D scaffold architecture, and that electrode had triple the areal loading of current slurry-based anodes.[28] As new directions like this appear for intermetallic alloys, the SnSb reported here may be useful for implementation in newer 3D architectures. Future studies in better understanding the structural integrity and electrochemistry that occur during cycling of this material may help improve not only the understanding and lifetime of SnSb, but hopefully of all intermetallic alloys that can lead to advancements towards commercialization.

This work was supported through the NSF SSMC program (SSMC-1710672). We would like to thank Ryan Weber (McCullagh Group, Dept. of Chemistry, Colorado State University) for help with creating a python code for analysing data. We also thank Dr Pat McCurdy, and Dr Brian Newell (Central Instrument Facility, Colorado State University) for their help with SEM and XRD experiments, respectively.

Conflicts of interest

The authors declare no competing financial interests.

Notes and references

1 P. Ge and M. Fouletier, *Solid State Ionics*, 1988, **28–30**, 1172–1175.
2 M. M. Doeff, Y. Ma, S. J. Visco and L. C. De Jonghe, *J. Electrochem. Soc.*, 1993, **140**, L169–L170.
3 D. A. Stevens and J. R. Dahn, *J. Electrochem. Soc.*, 2000, **147**, 1271–1273.
4 S. Komaba, Y. Matsuura, T. Ishikawa, N. Yabuuchi, W. Murata and S. Kuze, *Electrochem. Commun.*, 2012, **21**, 65–68.
5 C.-H. Lim, T.-Y. Huang, P.-S. Shao, J.-H. Chien, Y.-T. Weng, H.-F. Huang, B. J. Hwang and N.-L. Wu, *Electrochim. Acta*, 2016, **211**, 265–272.
6 C. M. Park and H. J. Sohn, *Electrochim. Acta*, 2009, **54**, 6367–6373.
7 F. J. Fernandez-Madrigal, P. Lavela, C. P. Vicente and J. L. Tirado, *Chem. Mater.*, 2002, **14**, 2962–2968.
8 L. G. Xue, X. Xia, T. Tucker, K. Fu, S. Zhang, S. L. Li and X. W. Zhang, *J. Mater. Chem. A*, 2013, **1**, 13807–13813.
9 M. Walter, S. Doswald and M. V. Kovalenko, *J. Mater. Chem. A*, 2016, **4**, 7053–7059.
10 Y. L. Li, W. Zhang, H. H. Cai, J. W. Wang, X. Z. Ren and P. X. Zhang, *RSC Adv.*, 2015, **5**, 105643–105650.
11 L. H. Shi, H. Li, Z. X. Wang, X. J. Huang and L. Q. Chen, *J. Mater. Chem.*, 2001, **11**, 1502–1505.
12 J. Yang, M. Winter and J. O. Besenhard, *Solid State Ionics*, 1996, **90**, 281–287.
13 J. O. Besenhard, J. Yang and M. Winter, *J. Power Sources*, 1997, **68**, 87–90.
14 H. P. Zhao, C. Y. Jiang, X. M. He and J. G. Ren, *J. Power Sources*, 2008, **184**, 532–537.
15 H. P. Zhao, G. Zhang, C. Y. Jiang and X. M. He, *Ionics*, 2012, **18**, 11–18.
16 Q. L. Jiang, D. Z. Hu, M. Q. Jia and R. S. Xue, *Appl. Surf. Sci.*, 2014, **321**, 109–115.
17 S. Sengupta, A. Patra, M. Akhtar, K. Das, S. B. Majumder and S. Das, *J. Alloys Compd.*, 2017, **705**, 290–300.
18 M. C. Schulze, R. K. Schulze and A. L. Prieto, *J. Mater. Chem. A*, 2018, **6**, 12708–12717.
19 X. Tang, Y. H. Wei, H. N. Zhang, F. L. Yan, M. Zhuo, C. M. Chen, P. Y. Xiao, J. J. Liang and M. Zhang, *Electrochim. Acta*, 2015, **186**, 223–230.
20 X. Tang, F. L. Yan, Y. H. Wei, M. Zhang, T. H. Wang and T. F. Zhang, *ACS Appl. Mater. Interfaces*, 2015, **7**, 21890–21897.
21 P. Antitomaso, B. Fraisse, M. T. Sougrati, F. Morato-Lallemand, S. Biscaglia, D. Ayme-Perrot, P. Girard and L. Monconduit, *J. Power Sources*, 2016, **325**, 346–350.
22 Z. Li, J. Zhang, J. Shu, J. Chen, C. Gong, J. Guo, L. Yu and J. Zhang, *J. Power Sources*, 2018, **381**, 1–7.
23 J. Qin, T. Wang, D. Liu, E. Liu, N. Zhao, C. Shi, F. He, L. Ma and C. He, *Adv. Mater.*, 2018, **30**, 1704670.
24 L. Baggetto, H. Y. Hah, J. C. Jumas, C. E. Johnson, J. A. Johnson, J. K. Keum, C. A. Bridges and G. M. Veith, *J. Power Sources*, 2014, **267**, 329–336.
25 A. Darwiche, M. T. Sougrati, B. Fraisse, L. Stievano and L. Monconduit, *Electrochem. Commun.*, 2013, **32**, 18–21.
26 M. Fehse, M. T. Sougrati, A. Darwiche, V. Gabaudan, C. La Fontaine, L. Monconduit and L. Stievano, *J. Mater. Chem. A*, 2018, **6**, 8724–8734.
27 H. Xie, X. Tan, E. J. Luber, B. Olsen, W. P. Kalisvaart, K. L. Jungjohann, D. Mitlin and J. M. Buriak, *ACS Energy Lett.*, 2018, **3**, 1670–1676.
28 P. Sun, J. Davis, L. Cao, Z. Jiang, J. B. Cook, H. Ning, J. Liu, S. Kim, F. Fan, R. G. Nuzzo and P. V. Braun, *Energy Storage Mater.*, 2019, **17**, 151–156.

